

pubs.acs.org/cm Article

# Highly Emissive Semi-Ladder-Type Copolymers, Aggregation State, and Solution-Processed Organic Light-Emitting Transistor

Dafei Yuan, Mohammad A. Awais, Valerii Sharapov, Xunshan Liu, Andriy Neshchadin, Wei Chen, and Luping Yu\*



**ACCESS** I

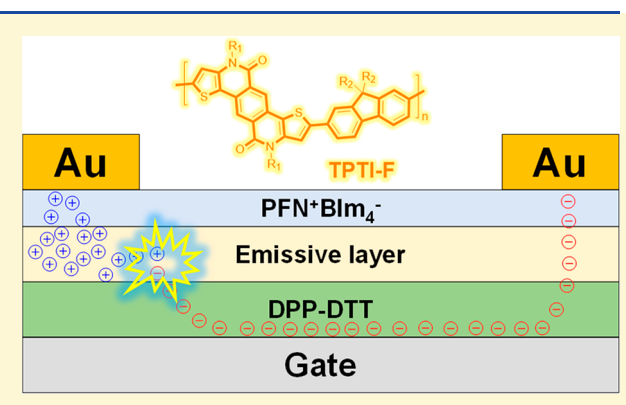
Cite This: Chem. Mater. 2020, 32, 4672-4680



Article Recommendations

ABSTRACT: An organic light-emitting transistor (OLET) integrates the logic function of a field-effect transistor (FET) with electroluminescence of a light-emitting diode (LED) into a single device. This has the potential to play an important role in smart displays, electrically pumped organic laser, and other flexible electronic devices. For achieving high-performance solution-processed OLET, three semiladder copolymers—TPTI-CC, TPTI-C, and TPTI-F—were developed. It was found that variation in the chemical structure lead to significant differences in energy level, emission color, and intermolecular aggregation. High photoluminescence quantum yields (PLQY) was obtained in these three polymers. Solution-processed trilayered OLET devices were fabricated, which exhibited strong electroluminescence, balanced charge mobility, and external quantum

Metrics & More



s Supporting Information

## **■** INTRODUCTION

efficiency (EQE) of 2.8%.

One of the success stories in the field of organic optoelectronics is that of the organic light-emitting diode which has already percolated from research laboratories to household electronics.<sup>1,2</sup> Another promising field is that of organic field-effect transistors (OFETs), which has the potential to morph into flexible devices.<sup>3–5</sup> Organic lightemitting transistor (OLET) combines both the electrical switching capability of OFETs and the light-generation capability of organic light-emitting diodes (OLEDs) in a single device, in which the intensity and recombination zone of electroluminescence (EL) can be effectively tuned by applying gate voltage.<sup>6-9</sup> A successful development of OLET technology can greatly simplify the display fabrication process and lead to new applications in electrically pumped organic lasers 10-13 and smart displays.<sup>14</sup> An efficient OLET should exhibit the following characteristics: a large  $I_{\rm on/off}$  ratio, a high charge mobility, a low applied voltage, a high external quantum efficiency (EQE), and tunable recombination zone.6-8 However, accomplishing all of the above remains a formidable task as current materials lack simultaneous ambipolar charge transport and strong luminescence in the solid-state. Moreover, effective ambipolar charge transport requires materials with highly ordered intermolecular stacking and proper matching of the highest occupied molecular orbital (HOMO) and lowest unoccupied molecular orbital (LUMO) energy levels with the Fermi energy level of metal electrodes. Unfortunately, strong intermolecular  $\pi$ – $\pi$  stacking will likely quench luminescence in

the solid-state. Thus, organic systems with high solid-state emission quantum yields generally exhibit less planar, but rigid structures, which necessarily impede charge transport and result in low charge carrier mobility.

To address this key issue, different types of materials have been developed, including small-molecules, polymers, singlecrystals, as well as charge-transfer (CT) cocrystals. 6,8,15-17 In 2003 Hepp and co-workers employed a bottom gate bottom contact (BGBC) device architecture to fabricate a tetracene based OLET device and observed light-emission. 9 Unfortunately, their device exhibited a very low EQE due to high charge injection energy barrier and low photoluminescent quantum yield (PLQY) of tetracene. 18 Later in 2006 Sirringhaus et al. used a fluorescent ambipolar semiconductor F8BT (PLQY = 60%) to fabricate asymmetric bottom contact top gate (BCTG) OLET device and achieved an impressive EQE of over 8%. 19,20 By precisely controlling the growth of single-crystals, both high PLQY, as well as high charge carrier mobility, can be achieved simultaneously in single-crystal devices. For instance, Hu et al. synthesized ambipolar semiconductors DPA and dNaAnt, exhibiting a balanced

Received: March 18, 2020 Revised: May 17, 2020 Published: May 18, 2020





electron/hole mobility of over  $10^{-1}~\rm cm^2~V^{-1}~s^{-1}$  and an EQE as high as 1.75% in single-crystal OLET devices with asymmetric electrodes. Park et al. developed a 2D slab CT cocrystal composed of 2MDCS ( $D_{\rm CT3}$ ) and CN-TFPA ( $A_{\rm CT3}$ ) and achieved an EQE of 1.5% in a simple BGBC OLET device with symmetric electrodes. However, the performance of OLET achieved up to date is still very low when in comparison with OLED. Moreover, the efficiency has recently plateaued due to a lack of high-performance fluorescent semiconductors that surpass F8BT.

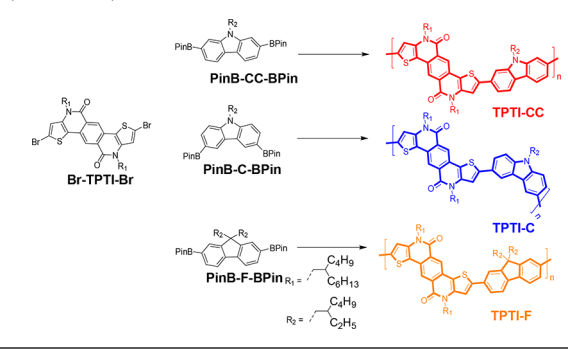
An alternative approach is to prepare multilayer devices, in which charge injection and charge-transporting layers are introduced.<sup>24–28</sup> In these multilayer devices, a high charge carrier mobility is not essential in the emissive layer provided that the energy levels are properly aligned and the solid-state emission quantum yield is high. This strategy was applied by Capelli et al. in their trilayered vacuum-deposition OLET device which exhibited balanced electron/hole mobility of 0.01 cm<sup>2</sup> V<sup>-1</sup> s<sup>-1</sup> and an EQE of 5%, more than 100 times higher than that of the equivalent OLED.<sup>24</sup> In 2020, Meng et al. used the thermally activated delayed fluorescence (TADF) smallmolecule materials and the hole transporting small-molecule C8-BTBT to construct trilayered OLET devices by vacuumdeposition, in which a peak EQE of 9.01% was achieved.<sup>28</sup> Though, these methods are not capable of solutionprocessability, which greatly limit their future application in printing electronics.

Thus, the development of new materials exhibiting proper energy level alignment, high PLQY, and solution-processed property has become critical for further progress in this area. In this work, we developed three weak donor-weak acceptor copolymers TPTI-CC, TPTI-C, and TPTI-F based on electron-deficient thieno[2',3':5,6]pyrido[3,4-g]thieno[3,2-c]isoquinoline-5,11(4H,10H)-dione (TPTI) and electron-rich fluorene and carbazoles. Here, carbazole (C) and fluorene (F) are weak electron-donating units and their homo/copolymers are highly fluorescent materials. 19,20,29-32 Ladder-type building TPTI, 34,35 is a fluorescent and weak electronwithdrawing group with good planarity and rigidity. It was found that the resulting three copolymers exhibit high PLQY and moderate charge carrier mobility. Moreover, solutionprocessed trilayered OLET devices based on these polymers were fabricated and exhibited high ambipolar charge mobility and strong electroluminescence. An excellent EQE of 2.8% was achieved in TPTI-F device, which is one of the highest among solution-processed OLETs (Table S1).

#### RESULTS AND DISCUSSION

The three copolymers (TPTI-CC, TPTI-C, and TPTI-F) were synthesized via the Suzuki coupling reaction as shown in Scheme 1. Here, TPTI-C is a cross-conjugated polymer while TPTI-F and TPTI-CC are fully conjugated. Thermogravimetric analysis (TGA) show high thermal stability in the three copolymers (Table 1). There is no peak observed in the DSC analysis indicating that no phase transition happens during thermal-annealing (Figure S1). Molecular weights ( $M_{\rm w}$ ) and the distribution are determined with gel permeation chromatography (GPC) as summarized in Table 1. All three polymers have good solubility in common organic solvents such as toluene, xylene, and chlorobenzene. DFT calculations at B3LYP level of theory using 6-31G\*\* basis set indicated a HOMO of -4.91 eV and a LUMO of -2.17 eV for TPTI-CC, which is slightly upshifted than the corresponding TPTI-F

Scheme 1. Synthesis of Ladder-Type Copolymers, TPTI-CC, TPTI-C, and TPTI-F



polymer (-4.93/-2.25 eV). TPTI-C exhibits a HOMO of -4.77 eV and a LUMO of -1.78 eV which is slightly higher than that of TPTI-CC. Our molecular geometry simulation clearly shows that TPTI-CC and TPTI-F exhibit linear polymer backbones (Figure 1). A coiled molecular backbone is formed in TPTI-C due to angled interconnection. From the cyclic voltammetry (CV) measurements (Figure S2), HOMO/LUMO energy levels of TPTI-CC, TPTI-C and TPTI-F were determined to be -5.20 eV/-3.20 eV, -5.11 eV /-3.09 eV, and -5.48 eV/-3.15 eV, respectively (Table 1). The slightly higher HOMO energy levels on TPTI-CC and TPTI-C should be attributed to the stronger electron-donating ability of carbazole than that of fluorene in TPTI-F.

The concentration-dependent UV-vis absorption spectra of TPTI-CC, TPTI-C, and TPTI-F are shown in Figure 2a-c. The three main absorption peaks at 480 nm (0-2), 514 nm (0-1) and 544 nm (0-0) are observed in the spectrum of TPTI-CC, which do not change with increasing concentration. In TPTI-CC thin film, the relative intensity of  $I_A^{0-1}/I_A^{0-2}$ decreases and the three peaks are significantly red-shifted to 496, 530, and 574 nm respectively. In the spectrum of TPTI-C, however, the solution absorption peaks at 447 nm (0-2), 478 nm (0-1), and 539 nm (0-0) remained unchanged with increasing concentration and are slightly red-shifted to 455, 486, and 554 nm in thin film. The relative peak intensity  $I_A^{0-0}/I_A^{0-1}$  shows no change, while the intensity ratio  $I_A^{0-1}/I_A^{0-2}$ decreases in solid-state. Moreover, for TPTI-F, there exist two main peaks at wavelengths of 460 (0-1) and 488 nm (0-0)and a minor shoulder peak in the solution absorption spectrum. The relative ratio of peak intensity  $I_A^{0-0}/I_A^{0-1}$ remained unchanged until the concentration reaches 0.05 mg/mL when the  $I_A^{0-0}/I_A^{0-1}$  ratio decreases. The thin film spectrum, however, is red-shifted to 468 and 498 nm, respectively.

Photoluminescence measurements provide further information to elucidate molecular aggregation. The emission spectrum of TPTI-CC film (Figure 2d) exhibits two peaks at 642 (0–0) and 712 nm (0–1) which are red-shifted from that of dilute solution (586 and 665 nm). Although the ratio of emission peak intensity (0-0)/(0-1) decreases as concentration increases, the 0–0 transition is still the dominant emission peak. This is consistent with the formation of Jaggregates in TPTI-CC. <sup>36</sup> In the emission spectrum of TPTI-C (Figure 2e), the emission peaks in dilute solution (0.001 mg/mL) are slightly red-shifted to 605 and 647 nm at higher concentration (0.1 mg/mL). The (0-0)/(0-1) ratio decreases gradually with increasing concentration and the 0–0 transition is almost totally suppressed in the solid-state,

Table 1. Chemical Property of TPTI-CC, TPTI-C and TPTI-F

	HOMO (eV)	LUMO (eV)	$E_{ m g}^{ m film}~({ m eV})$	$E_{\rm g}^{ m solution}$ (eV)	PLQY (%)	$M_{ m w}$	$M_{\rm n}$	PDI	$T_{\rm d} ({}^{\circ}{\rm C})^{d}$
TPTI-CC	$-5.20^{b} (-4.91)^{a}$	$-3.20^{c} (-2.17)^{a}$	2.00	2.11	23	32 428	23 471	1.38	340
TPTI-C	$-5.11^{b} (-4.77)^{a}$	$-3.09^{c} (-1.78)^{a}$	2.02	2.14	21	17 797	14 070	1.26	320
TPTI-F	$-5.48^{b} (-4.93)^{a}$	$-3.15^{c} (-2.25)^{a}$	2.33	2.43	59	11 963	9421	1.27	370

"Calculated from DFT. "Calculated from oxidation onset of CV spectra.  $^cE_{\text{LUMO}} = E_{\text{HOMO}} + E_{\text{g}}^{\text{film}}$ . "TGA data showing the temperature for onset of 5% mass loss.

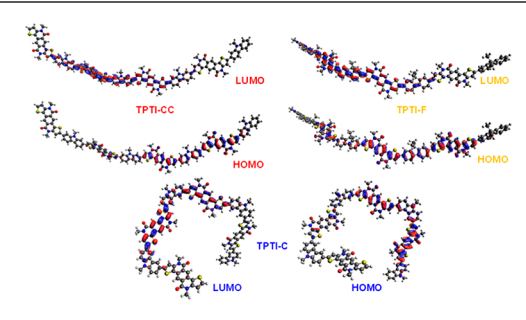


**Figure 1.** Calculated HOMO and LUMO molecular orbital distribution of TPTI-CC, TPTI-C, and TPTI-F.

which may be attributed to H-aggregation.<sup>36</sup> As shown in the emission spectrum of TPTI-F (Figure 2f), the intensity of 0-0 (500 nm) emission decreases significantly with increasing concentration and nearly vanishes in thin film. The prevention of 0–0 emission and decreased  $I_A^{0-0}/I_A^{0-1}$  ratio in absorption imply strong H-aggregation in TPTI-F films.<sup>36</sup> The thin-film photoluminescence spectra of TPTI-F (Figure 2f) shows a major emission peak at 582 nm and a shoulder peak at around 619 nm which is significantly red-shifted from that in dilute solution. The red-shifted H-aggregates of TPTI-F and TPTI-C are similar to quadrupolar dyes. 37,38 Besides, the 0-0 and 0-1 emission peaks in solution are almost completely suppressed in thin film. The large redshift and almost featureless shape in solid-state photoluminescent spectra seems to indicate the formation of excimer due to strong interchain interaction in TPTI-F.<sup>39</sup> Interestingly, TPTI-CC and TPTI-C showed only moderate PLQY of 23% and 21% respectively in chloroform solution with a concentration of 0.001 mg/mL (Table 1), while TPTI-F exhibited PLQY of 59% which was nearly three

times higher. To gain more insight into the photophysical properties, time-resolved fluorescence decay is measured for polymer solutions (Table S2). Fluorescence decay curves are fitted with exponential decay equation and fluorescence lifetimes were calculated. It is found that polymer TPTI-F exhibits the longest fluorescence lifetime of 1.06 ns at the highest concentration with a single exponential decay behavior. TPTI-C and TPTI-CC exhibit double exponential decay which may indicate the presence of different relaxation pathways.

Grazing-incidence wide-angle X-ray scattering (GIWAXS) studies indicated that TPTI-C and TPTI-F exhibit weak crystallinity with less tight molecular packing ( $d_{\pi-\pi}=3.9$  Å in TPTI-C;  $d_{\pi-\pi}=4.1$  Å in TPTI-F). This is consistent with Haggregation in which branched alkyl chains on TPTI moiety closely contact (Figure 3b–e). TPTI-CC, however, exhibits enhanced lamellar stacking along the in-plane direction (Figure 3e) and more tightly  $\pi-\pi$  stacking ( $d_{\pi-\pi}=3.6$  Å; Figure 3a,d). This is consistent with its more planar molecular backbone, higher  $M_{\rm w}$  and J-aggregation.

To investigate the electronic properties of the three polymers, bottom gate top contact (BGTC) FET devices were fabricated. Silicon dioxide (SiO<sub>2</sub>) with a thickness of ~300 nm was used as the dielectric layer, on which a self-assembled n-octadecyltrichlorosilane (OTS) monolayer was immobilized to reduce charge trapping caused by the surface hydroxyl groups. After coating the polymer solutions on the substrate under N<sub>2</sub> atmosphere, the films were thermally annealed for half an hour on a hot-plate at an optimized temperature of 120 °C. Gold (Au) was then vacuum deposited on the active layers as drain and source electrodes through a mask with the channel length of 50  $\mu$ m and channel width of 18 mm. FET devices for TPTI-CC show unipolar transport

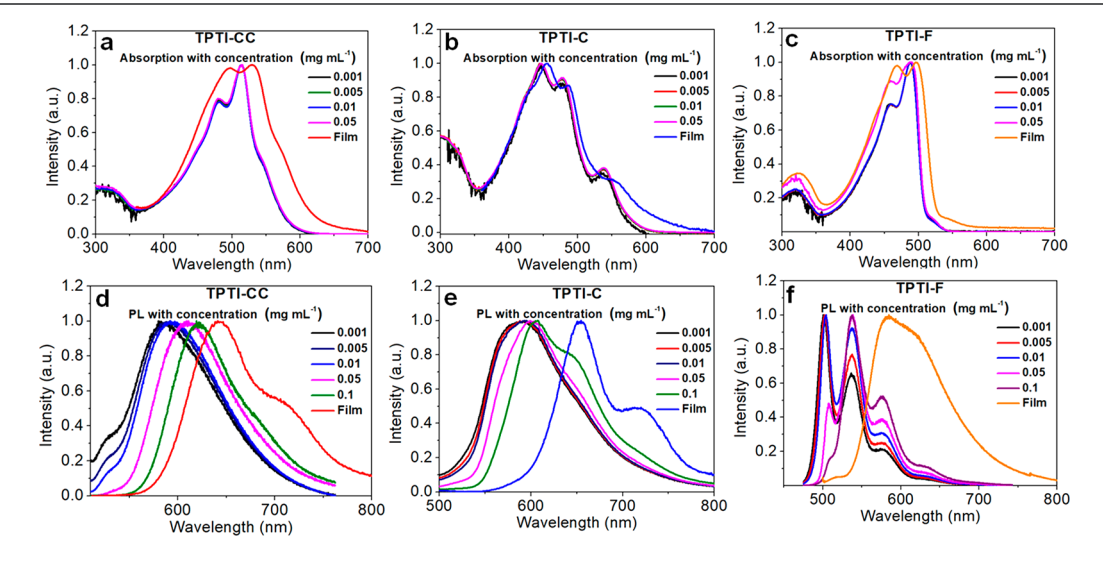


Figure 2. Concentration-dependent UV—vis absorption spectra (a-c), and photoluminescence (PL) spectra (d-f) of TPTI-CC, TPTI-C, and TPTI-F in chloroform solution and thin film, respectively.

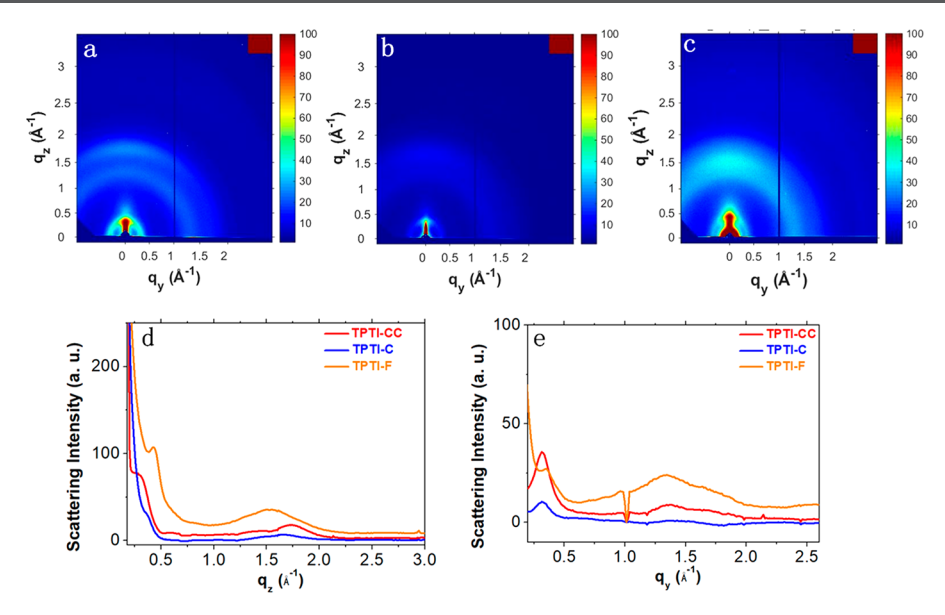


Figure 3. 2D GIWAXS images of (a) TPTI-CC, (b) TPTI-C, and (c) TPTI-F. 1D GIWAXS linecut along out-of-plane (d) and in-plane (e) directions.

behavior with moderate hole mobility of  $3.1 \times 10^{-4}$  cm<sup>2</sup> V<sup>-1</sup> s<sup>-1</sup> and  $I_{\text{on/off}}$  ratio of  $10^2$  (Figure S3a and Table 2). Much

Table 2. Electrical Property Measured from FET and OLET Devices of TPTI-CC, TPTI-C, and TPTI-F

	$\mu_{\rm h} \; ({\rm cm^2 \; V^{-1} \; s^{-1}}) \; [{\rm max \; (avg)}]$	$\mu_{\rm e} \; ({\rm cm^2 \; V^{-1} \; s^{-1}}) \ [{\rm max \; (avg)}]$	$I_{ m on/off}$ [max (avg)]
TPTI-CC <sup>a</sup>	$3.1 \times 10^{-4} $ $(2.7 \times 10^{-4})$		$10^2 (10^2)$
TPTI-C <sup>a</sup>		$1.9 \times 10^{-6}$ $(1.5 \times 10^{-6})$	$10^1 (10^1)$
TPTI-F <sup>a</sup>		$1.8 \times 10^{-6} $ $(1.1 \times 10^{-6})$	10 <sup>1</sup> (10 <sup>1</sup> )
TPTI-CC <sup>b</sup>	0.041 (0.036)	0.059 (0.053)	$10^3/10^2 \left(10^3/10^2\right)$
TPTI-C $^b$	0.39 (0.30)	0.23 (0.18)	$10^4/10^4 \left(10^4/10^3\right)$
$TPTI-F^{b}$	0.051 (0.046)	0.014 (0.011)	$10^4/10^4 \left(10^4/10^3\right)$
TPTI-CC <sup>€</sup>	0.26 (0.22)	0.024 (0.018)	$10^5/10^4 \left(10^4/10^3\right)$
TPTI- $C^c$	0.024 (0.018)	0.016 (0.013)	$10^4/10^3 \left(10^3/10^3\right)$
TPTI-F <sup>c</sup>	0.044 (0.038)	0.046 (0.040)	$10^5/10^4 \left(10^4/10^4\right)$
$DPP\text{-}DTT^b$	0.086 (0.074)	0.048 (0.043)	$10^3/10^3 \left(10^3/10^2\right)$
$DPP\text{-}DTT^c$	0.96 (0.80)	0.34 (0.25)	$10^6/10^4 \left(10^6/10^4\right)$

"Mobility calculated from OTS modified OFET devices. <sup>b</sup>Mobility calculated from OLET devices with PMMA as modification layer. <sup>c</sup>Mobility calculated from OTS modified OLET devices.

lower electron mobility of  $1.5 \times 10^{-6}$  cm $^2$  V $^{-1}$  s $^{-1}$  and a small  $I_{\rm on/off}$  of  $10^1$  is obtained for TPTI-C with coiled structure (Figure S3b). FET devices for TPTI-F, however, were unipolar in which only n-type transfer curves were observed. Low electron mobility of  $1.8 \times 10^{-6}$  cm $^2$  V $^{-1}$  s $^{-1}$  and a small  $I_{\rm on/off}$  of  $10^1$  was obtained (Table 2). The relatively higher charge carrier mobility of TPTI-CC is consistent with J-aggregation as well as enhanced lamellar stacking and more tightly  $\pi$ - $\pi$  stacking as shown in GIWAXS (Figure 3). Although both FET charge transport, as well as high PLQY, were achieved in TPTI-CC, TPTI-C, and TPTI-F, no electroluminescence was observed in these single-layered OFET devices. This might be related to the high injection energy barrier and low charge mobility that limits the hole and electron recombination in the

emissive layer as a consequence of long channel length (50  $\mu m$ ).

To address the issue of charge injection and low charge mobility, we fabricated solution-processed trilayered OLET devices as shown in Figure 4a. 25,26 Poly(methyl methacrylate)

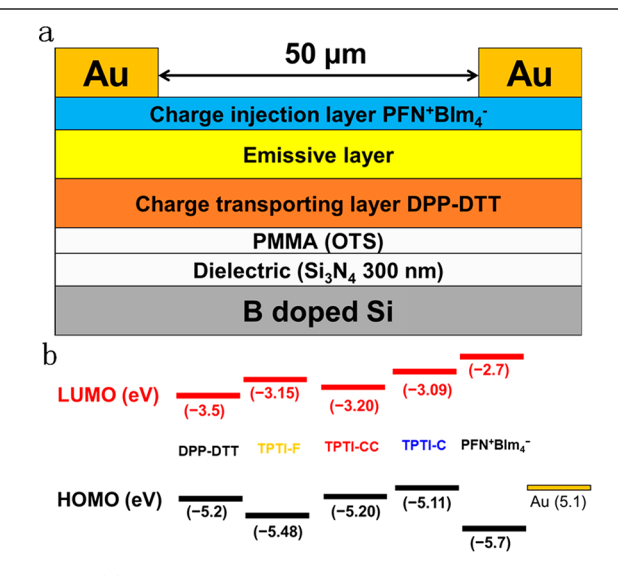


Figure 4. (a) Device configuration of OLET: B doped Si as gate electrode,  $Si_3N_4$  as dielectric layer, a thick poly(methyl methacrylate) (PMMA) film or self-assemble monolayer OTS as modification layer on  $Si_3N_4$ ; DPP-DTT work as transporting layer; PFN $^{\dagger}$ BIm $_4^-$  as electron injection layer, symmetric gold electrode as drain and source; (b) the energy diagram for OLET devices.

(PMMA) in propyl acetate with a concentration of 30 mg/mL was spin-coated on top of  $\mathrm{Si_3N_4}$ , with a thickness of around 120–150 nm, to reduce charge trapping. The commercially available semiconducting polymer DPP-DTT in chloroform solution (5 mg/mL) was spin-coated on PMMA as the charge transporting layer. DPP-DTT exhibited both high electron and high hole mobility (Table 2). As shown in Figure 4b, the highlying HOMO (–5.2 eV) and low-lying LUMO (–3.5 eV) on DPP-DTT match well with the emissive layer, which should

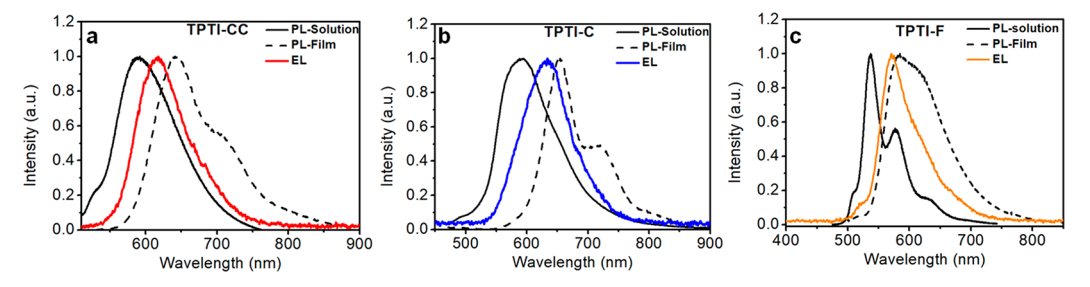


Figure 5. Electroluminescent (EL) and photoluminescent (PL) spectra of TPTI-CC (a), TPTI-C (b), and TPTI-F (c).

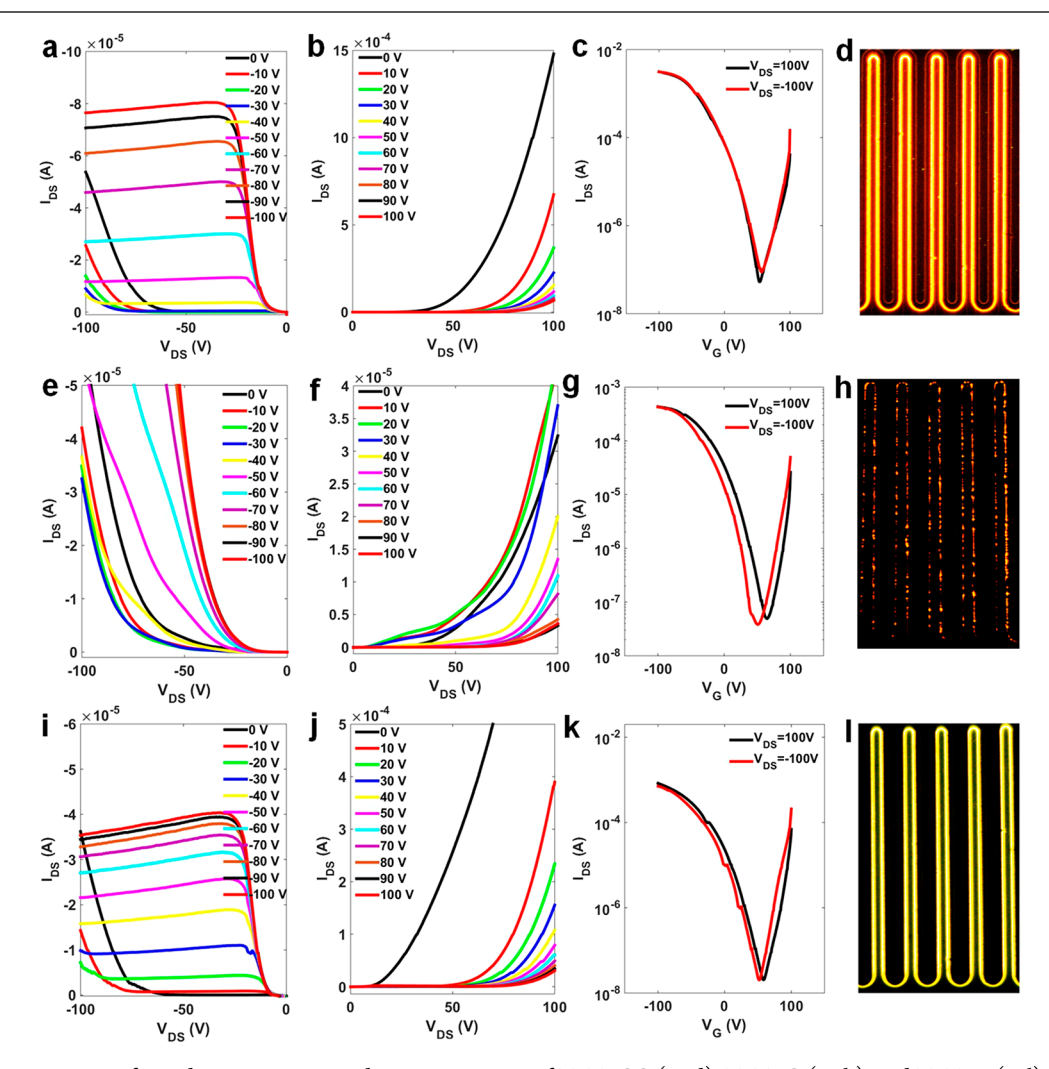


Figure 6. Characteristic transfer and output curves, and emission images of TPTI-CC (a–d), TPTI-C (e–h), and TPTI-F (i–l) in BGTC OLET with optimized device configuration as shown in Figure 4a (OTS as modification layer). Channel length,  $L = 50 \mu m$ ; channel width, W = 18 mm.

facilitate the hole or electron transport from DPP-DTT to the emissive layer. DPP-DTT has poor solubility in xylene or toluene, which makes it feasible to fabricate the whole OLET device through solution-processing. The emissive polymer in xylene solution (12 mg/mL) was deposited on the top of DPP-DTT by spin-coating. From the energy level diagram (Figure 4b), we can find that the LUMO of TPTI-CC, TPTI-C, and TPTI-F is aligned rather high relative to the work function ( $W_F \approx 5.1 \text{ eV}$ ) of Au, which will impede electron injection. Therefore, conjugated polyelectrolyte (CPE), PFN+BIm<sub>4</sub> was used as the electron-injection layer because its unique ionic effect can lower the electron injection energy barrier. Methanol was used as the solvent for PFN+BIm<sub>4</sub> to avoid dissolution of

the emissive layer underneath. As demonstrated before, the thickness of PFN $^{+}BIm_{4}^{-}$  plays an important role in the performance of OLET.  $^{25}$  After both the concentration and the spin-rate of PFN $^{+}BIm_{4}^{-}$  were optimized, it was found that PFN $^{+}BIm_{4}^{-}$  with a thickness lower than 10 nm is optimal in our OLET devices. Then, Au with a thickness of 30 nm were deposited on top of PFN $^{+}BIm_{4}^{-}$  as symmetric drain-source electrodes. At least ten OLET devices were fabricated and tested for each emissive polymer.

As shown in Figure S4, our OLET devices of TPTI-CC, TPTI-C, and TPTI-F exhibit ambipolar FET behavior with hole/electron mobility of 0.041/0.059, 0.39/0.23, and 0.051/0.014 cm $^2$  V $^{-1}$  s $^{-1}$  respectively (Table 2). The  $I_{\rm on/off}$  ratio of

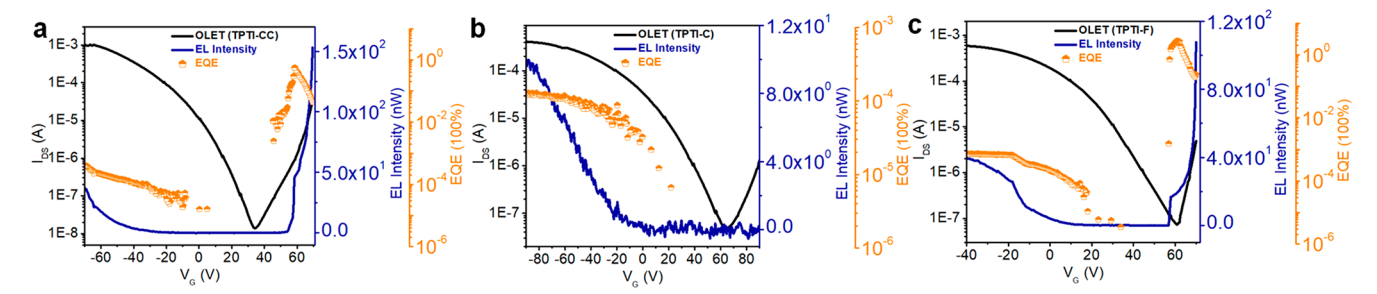


Figure 7. Source-drain current,  $I_{\rm DS}$  (black), electroluminescent (EL) intensity (blue), and EQE (orange) change with gate voltages of OTS modified OLET devices: TPTI-CC,  $V_{\rm DS}$  = 70 V (a), TPTI-C,  $V_{\rm DS}$  = 90 V (b), and TPTI-F,  $V_{\rm DS}$  = 70 V (c).

TPTI-C and TPTI-F are significantly improved from 10<sup>1</sup> to 10<sup>4</sup>. This greatly improved FET property should be attributed to the incorporation of DPP-DTT as a charge transporting layer. Yellow-orange, orange, and yellow emission were observed for TPTI-CC, TPTI-C, and TPTI-F respectively, as shown in Figure S4d,h,l. The EL spectra of TPTI-CC and TPTI-C were blue-shifted relative to PL spectra in solid-state, which might imply that the EL came from relatively less aggregated emissive centers (Figure 5a,b). The electroluminescent spectra of TPTI-F exhibited a main peak at around 572 nm (Figure 5c) which was close to the PL spectra in film (582 nm). Although large drain-source and gate voltages were applied, the performances of OLET with this architecture was still poor. The low intensity and narrow emission zone may be attributed to the poor FET transporting property of DPP-DTT on PMMA (Table 2).

In order to further improve device performances, we employed self-assembled OTS monolayer to replace the thick insulating PMMA layer (Figure 4a). As shown in Figure 6, emission from these devices is significantly stronger than the emission from PMMA modified ones. Interestingly, the emission regions of TPTI-CC and TPTI-F are extending further from electrodes than that of TPTI-C under the same gate voltage.

The emissions are still fixed near the electrodes, which are possibly attributed to the poor charge transporting property of PFN<sup>+</sup>BIm<sub>4</sub><sup>-</sup> and emissive layer, and OLED-like working mode. Moreover, the  $I_{\rm on/off}$  ratio of TPTI-CC and TPTI-F OLET devices increases significantly than before as shown in Table 2. These improvements may be partially attributed to the enhancement of charge transport in the OLET devices of TPTI-CC and TPTI-F. GIWAXS studies indicate significantly enhanced diffraction peak intensity at q=0.3 and 0.6 Å<sup>-1</sup> along the out-of-plane direction and q=0.1 Å<sup>-1</sup> along the inplane direction of DPP-DTT films on OTS modified devices in comparison with those on PMMA (Figure S5). As shown in Table 2 and Figures S6 and S7, both charge carrier mobility and  $I_{\rm on/off}$  ratio of DPP-DTT on OTS modified FET devices were enhanced significantly in comparison with that on PMMA

We used a photodetector to measure the photocurrent and calculated the electroluminescent outpower (EL intensity) and EQE of these OLET devices, after calibrating with OLED of the same material. As shown in Figure 7a, the EL intensity for TPTI-CC increase from 0.5 nW ( $V_{\rm G}=-20~{\rm V}$ ) to 26 nW ( $V_{\rm G}=-65~{\rm V}$ ), which is consistent with the device switching-on at  $-20~{\rm V}$  and increased emission intensity as  $V_{\rm G}$  is increased. From  $V_{\rm G}=55~{\rm to}~70~{\rm V}$ , the EL intensity increases significantly from 4 to 153 nW, which is comparable to the vacuum-deposited trilayered OLET device. Based on the

number of photons and electrons from drain-source current, the EQE of TPTI-CC was calculated, as shown in Figure 7a as a function of V<sub>G</sub>. The highest EQE was determined to be 0.56% at low applied voltages:  $V_{\rm G}$  = 59 V and  $V_{\rm DS}$  = 70 V. In contrast with TPTI-CC, a relatively lower EL intensity (9 nW at  $V_G = -80 \text{ V}$ ) is obtained in TPTI-C (Figure 7b), though a larger voltage is applied. The large drain-source current and a lower photon count makes the EQE of TPTI-C (0.00013%) at  $V_G = -80 \text{ V}$  and  $V_{DS} = 90 \text{ V}$ , 3 orders of magnitude lower than that of TPTI-CC. As shown in Figure 7c, the EL intensity of TPTI-F increases from 0.07 nW ( $V_G = 35 \text{ V}$ ) to 40 nW ( $V_G = 35 \text{ V}$ ) to 40 nW ( $V_G = 35 \text{ V}$ ) -40 V). From  $V_G = 58$  to 70 V, the EL intensity increased significantly from 16.9 to 108 nW. The EQE of TPTI-F was calculated as shown in Figure 7c. The highest EQE was determined to be 2.8% at low applied voltages:  $V_G = 62 \text{ V}$  and  $V_{\rm DS} = 70$  V, which is five times higher than that of TPTI-CC. Notably, more than 1000 times higher EQE are achieved in OLET in comparison with the corresponding trilayer OLED (ITO/PEDOT:PSS/DPP-DTT/emissive layer/PFN+BIm<sub>4</sub>-/ Ca/Al) as shown in Figure S8, which demonstrate the great potential in trilayered OLETs for flexible organic electronic

The low performance of TPTI-C may be attributed to the weak crystallinity and poor charge transporting property due to its coiled structure, which limits the transport and recombination of charge carriers in the TPTI-C emissive layer. Moreover, significantly low PLQY in TPTI-C also results in low EQE. In comparison, the planar molecular backbone, strong crystallinity and matched energy level of TPTI-CC will facilitate the injection of charge carriers from the electrodes and allow their recombination in the emissive layer. However, the intrinsically low PLQY in TPTI-CC and unbalanced charge mobility on OTS modified OLET devices leads to the relatively lower EQE in comparison with TPTI-F.

## CONCLUSION

We designed and synthesized three semiladder-type copolymers, TPTI-CC, TPTI-C, and TPTI-F. The structural variations in TPTI-CC, TPTI-C, and TPTI-F dictates their different aggregation states and electronic effects. These three polymers exhibit good emission, suitable energy levels, and decent FET behavior. By carefully selecting the electron injection, charge transporting and modification layers, high-performance solution-processed trilayered OLETs were prepared. The high PLQY in TPTI-F and balanced electron and hole mobility of 0.046 and 0.044 cm² V $^{-1}$  s $^{-1}$  obtained in TPTI-F based trilayered OLET devices, contribute to an EQE as high as 2.8% even at a relatively low voltages ( $V_{\rm G}=62$  V and  $V_{\rm DS}=70$  V). Further improvement of the intrinsically charge

mobility in TPTI-F without sacrifice of PLQY through molecular engineering, should lead to higher device performance.

#### EXPERIMENTAL SECTION

Fabrication of OLET Devices. Devices were assembled in bottom gate top contact (BG-TC) configuration. B doped silicon wafers with 300 nm silicon nitride were purchased from University Wafers and used as substrates. Wafers were cut into 14 × 19 mm slides and ultrasonicated in acetone and isopropanol for 15 min each. After that they were dried using compressed dry nitrogen. Silicon wafers were modified with octadecyltrichlorosilane (OTS). For OTS modification, silicon wafers were put in glass Petri dish and one drop of OTS were added. It was kept in vacuum oven at 120 °C for 1 h. The solution of DPP-DTT was spin-coated on rotating substrate at 1500 rpm/60 s and annealed at 120 °C for 30 min in glovebox. Active layer polymers were dissolved in p-xylene with the concentration 10 mg mL-1 and spin-coated on DPP-DTT at 2000 rpm for 40 s. Polymer films were annealed at 120 °C for 30 min in glovebox. PFN+BIm<sub>4</sub> was dissolved in methanol with the concentration of 2 mg mL<sup>-1</sup>. After filtration, PFN<sup>+</sup>BIm<sub>4</sub><sup>-</sup> was spin-coated on active layer at 7000 rpm for 30 s. Polymer films were annealed at 60 °C for 20 min in air and transferred back to glovebox for thermal deposition of source-drain electrodes. Thirty nm of gold was deposited in vacuum chamber under pressure <10<sup>-6</sup> Torr through a shadow mask purchased from Ossila Ltd.

Characterization of OLET Devices. All devices were tested in nitrogen glovebox in dark. Two-channel SMU Keithley 2612A was used to test output and transfer characteristics of devices. Electroluminescence spectra of emissive polymers were obtained from OLED devices. The structure of the OLED devices was ITO/PEDOT:PSS/ DPP-DTT/emissive layer/PFN+BIm<sub>4</sub>-/Ca/Al. ITO glasses were ultrasonicated in chloroform, acetone and isopropanol for 15 min each and dried using compressed nitrogen. Glasses were cleaned in UV/ozone for 20 min. PEDOT:PSS from Heraeus was spin-coated on ITO at 6000 rpm for 60 s and annealed in vacuum oven at 95 °C. A solution of emissive layer in p-xylene with the concentration 12 mg mL<sup>-1</sup> was spin-coated on PEDOT:PSS at 1500 rpm for 30 s and annealed at 100 °C for 30 min in glovebox. Then 20 nm calcium and 80 nm aluminum were thermally evaporated in vacuum chamber under pressure <10<sup>-6</sup> Torr through a shadow mask that defined the device area of 3.14 mm<sup>2</sup>. Electroluminescence spectra of these OLEDs were measured using a calibrated integrating sphere AvaSphere-50-IRRAD and AvaSpec-ULS2048 spectrometer from Avantes and source meter unit Keithley 2420 to drive OLED.

**EQE Measurements.** In order to measure EQE of OLET devices we used a modified method previously described elsewhere. The photodiode FDS100-CAL purchased from Thorlabs was calibrated with OLED of known irradiance based on the same emissive layer as OLET. The irradiance of OLED was measured using calibrated integrating sphere AvaSphere-50-IRRAD and AvaSpec-ULS2048 spectrometer. Photocurrent from the calibrated photodiode placed right in front of the operating device was used to calculate brightness of OLET devices and based on it calculate photon flux. Lambertian emission was assumed. The number of electrons injected in the device was calculated from source drain current. EQE was calculated as the ratio of photon flux to the number of injected electrons per second.

GIWAXS Analysis. The GIWAXS measurements were performed at 8ID-E beamline of Advanced Photon source Argonne National Laboratory with the radiation wavelength 1.1354 Å. Samples were prepared on polished silicon wafer covered with PEDOT: PSS. The same solvent and annealing mode were used as in the actual device fabrication process.

Synthesis of Semiladder Copolymers. General Procedure. A mixture of Br-TPTI-Br monomer (1 equiv) and carbazole/fluorene comonomer (1 equiv),  $K_2CO_3$  (4 equiv), Aliquat 336 (3 drops), and  $Pd(PPh_3)_4$  (0.05 equiv) were dissolved in 4 mL of toluene/ $H_2O$  (10:1). The mixture was degassed for 30 min and then refluxed for 72 h. After cooling to room temperature, the mixture was passed through

Celite and precipitated in methanol. The polymer fibers were then washed by Soxhlet extraction with methanol, acetone, hexanes, and chloroform. The final polymer was obtained after reprecipitation of chloroform fraction in methanol.

TPTI-CC. A mixture of Br-TPTI-Br (0.200g, 0.244 mmol), PinB-CC-BPin (0.130g, 0.244 mmol),  $K_2CO_3$  (0.135g, 0.977 mmol), Aliquat 336 (3 drops), and Pd(PPh<sub>3</sub>)<sub>4</sub> (0.014g, 0.012 mmol) were dissolved in 6 mL of toluene/H<sub>2</sub>O (10:1). The mixture was degassed for 30 min and then refluxed for 72 h. After cooling to room temperature, the mixture was added to methanol. The precipitate was dissolved in chloroform and filtered with Celite. The polymer fibers were then washed by Soxhlet extraction with methanol, acetone, hexanes, and chloroform. The final polymer was obtained after reprecipitation in methanol as red solid. Yield: 89%. <sup>1</sup>H NMR (500 MHz,  $C_2D_2Cl_4$ ): δ (ppm) 6.6–9.0 (br, 10H), 3.60–4.85 (br, 6H), 2.0–2.35 (br, 3H), 1.15–1.75 (m, 40H), 0.72–1.11 (m, 18H). Elemental Analysis calculated for [ $C_{60}H_{79}N_3O_2S_2$ ]n: C: 76.79; H: 8.49; N: 4.48. Found: C: 75.39; H: 8.17; N: 4.13.

*TPTI-C.* A mixture of Br-TPTI-Br (0.200g, 0.244 mmol), PinB-C-BPin (0.130g, 0.244 mmol),  $K_2CO_3$  (0.135g, 0.977 mmol), Aliquat 336 (3 drops), and Pd(PPh<sub>3</sub>)<sub>4</sub> (0.014g, 0.012 mmol) were dissolved in 6 mL of toluene/ $H_2O$  (10:1). The mixture was degassed for 30 min and then refluxed for 72 h. After cooling to room temperature, the mixture was added to methanol. The precipitate was dissolved in chloroform and filtered with Celite. The polymer fibers were then washed by Soxhlet extraction with methanol, acetone, hexanes, and chloroform. The final polymer was obtained after reprecipitation in methanol as red solid. Yield: 88%. <sup>1</sup>H NMR (500 MHz,  $C_2D_2Cl_4$ ): δ (ppm) 6.6–9.0 (br, 10H), 3.50–5.20 (br, 6H), 1.98–2.34 (br, 3H), 1.16–1.74 (m, 40H), 0.72–1.11 (m, 18H). Elemental Analysis calculated for [ $C_{60}H_{79}N_3O_2S_2$ ]n: C: 76.79; H: 8.49; N: 4.48. Found: C: 75.46; H: 8.47; N: 4.28.

*TPTI-F.* A mixture of Br-TPTI-Br (0.200g, 0.244 mmol), PinB-F-BPin (0.157g, 0.244 mmol),  $K_2CO_3$  (0.135 g, 0.977 mmol), Aliquat 336 (3 drops), and Pd(PPh<sub>3</sub>)<sub>4</sub> (0.014g, 0.012 mmol) were dissolved in 6 mL of toluene/ $H_2O$  (10:1). The mixture was degassed for 30 min and then refluxed for 72 h. After cooling to room temperature, the mixture was added to methanol. The precipitate was dissolved in chloroform and filtered with Celite. The polymer fibers were then washed by Soxhlet extraction with methanol, acetone, hexanes, and chloroform. The final polymer was obtained after reprecipitation in methanol as orange solid. (yield: 82%). <sup>1</sup>H NMR (500 MHz, CDCl<sub>3</sub>):  $\delta$  (ppm) 8.92 (s, 2H) 7.30–8.01 (br, 8H), 4.33 (br, 4H), 2.14 (br, 6H), 1.20–1.51 (m, 32H), 0.61–1.05 (m, 42H). Elemental Analysis calculated for [ $C_{69}H_{96}N_2O_2S_2$ ]n: C: 78.96; H: 9.22; N: 2.67. Found: C: 77.63; H: 9.06; N: 2.69.

## ASSOCIATED CONTENT

# Supporting Information

The Supporting Information is available free of charge at https://pubs.acs.org/doi/10.1021/acs.chemmater.0c01168.

Cyclic voltammetry (CV) curves, DSC analysis, fabrication and characterization of FET, GIWAXS, and concentration-dependent fluorescence lifetimes (PDF)

#### AUTHOR INFORMATION

# **Corresponding Author**

Luping Yu — Department of Chemistry and the James Franck Institute, The University of Chicago, Chicago, Illinois 60637, United States; Email: lupingyu@uchicago.edu

#### **Authors**

Dafei Yuan − Department of Chemistry and the James Franck Institute, The University of Chicago, Chicago, Illinois 60637, United States; oorcid.org/0000-0001-5914-2060

- **Mohammad A. Awais** Department of Chemistry and the James Franck Institute, The University of Chicago, Chicago, Illinois 60637, United States
- Valerii Sharapov Department of Chemistry and the James Franck Institute, The University of Chicago, Chicago, Illinois 60637, United States; oorcid.org/0000-0002-2828-0468
- Xunshan Liu − Department of Chemistry and the James Franck Institute, The University of Chicago, Chicago, Illinois 60637, United States; oorcid.org/0000-0003-1537-258X
- Andriy Neshchadin Department of Chemistry and the James Franck Institute, The University of Chicago, Chicago, Illinois 60637, United States; orcid.org/0000-0002-8548-1186
- Wei Chen Materials Science Division, Argonne National Laboratory, Lemont, Illinois 60439, United States

Complete contact information is available at: https://pubs.acs.org/10.1021/acs.chemmater.0c01168

#### **Author Contributions**

§These authors contributed equally.

#### **Notes**

The authors declare no competing financial interest.

## ACKNOWLEDGMENTS

This work was supported by NSF (Chem-1802274, L.P.Y.), partially supported by the University of Chicago Materials Research Science and Engineering Center, which is funded by the National Science Foundation under Award No. DMR-1420709. We also thank Dr. Joseph Strzalka and Dr. Zhang Jiang for the assistance with GIWAXS measurements. This research used resources of the Advanced Photon Source, a U.S. Department of Energy (DOE) Office of Science User Facility operated for the DOE Office of Science by Argonne National Laboratory under Contract No. DE-AC02-06CH11357.

#### REFERENCES

- (1) Zhang, D.; Huang, T.; Duan, L. Emerging Self-Emissive Technologies for Flexible Displays. *Adv. Mater.* **2020**, 32, No. 1902391.
- (2) Heeger, A. J. Semiconducting and Metallic Polymers: The Fourth Generation of Polymeric Materials (Nobel Lecture). *Angew. Chem., Int. Ed.* **2001**, *40*, 2591–2611.
- (3) Sirringhaus, H. 25th Anniversary Article: Organic Field-Effect Transistors: The Path Beyond Amorphous Silicon. *Adv. Mater.* **2014**, 26, 1319–35.
- (4) Zhao, Y.; Guo, Y.; Liu, Y. 25th Anniversary Article: Recent Advances in N-Type and Ambipolar Organic Field-Effect Transistors. *Adv. Mater.* **2013**, *25*, 5372–91.
- (5) Ren, Y.; Yang, X.; Zhou, L.; Mao, J. Y.; Han, S. T.; Zhou, Y. Recent Advances in Ambipolar Transistors for Functional Applications. *Adv. Funct. Mater.* **2019**, 29, 1902105.
- (6) Zhang, C.; Chen, P.; Hu, W. Organic Light-Emitting Transistors: Materials, Device Configurations, and Operations. *Small* **2016**, *12*, 1252–94
- (7) Liu, C. F.; Liu, X.; Lai, W. Y.; Huang, W. Organic Light-Emitting Field-Effect Transistors: Device Geometries and Fabrication Techniques. *Adv. Mater.* **2018**, *30*, No. 1802466.
- (8) Zaumseil, J. Recent Developments and Novel Applications of Thin Film, Light-Emitting Transistors. *Adv. Funct. Mater.* **2020**, *30*, 1905269.
- (9) Hepp, A.; Heil, H.; Weise, W.; Ahles, M.; Schmechel, R.; von Seggern, H. Light-Emitting Field-Effect Transistor Based on a Tetracene Thin Film. *Phys. Rev. Lett.* **2003**, *91*, 157406.
- (10) Toffanin, S.; Capelli, R.; Koopman, W.; Generali, G.; Cavallini, S.; Stefani, A.; Saguatti, D.; Ruani, G.; Muccini, M. Organic Light-

Emitting Transistors with Voltage-Tunable Lit Area and Full Channel Illumination. *Laser & Photonics Reviews* **2013**, *7*, 1011–1019.

- (11) Koopman, W. A.; Natali, M.; Donati, G. P.; Muccini, M.; Toffanin, S. Charge–Exciton Interaction Rate in Organic Field-Effect Transistors by Means of Transient Photoluminescence Electromodulated Spectroscopy. *ACS Photonics* **2017**, *4*, 282–291.
- (12) Sandanayaka, A. S. D.; Matsushima, T.; Bencheikh, F.; Terakawa, S.; Potscavage, W. J.; Qin, C.; Fujihara, T.; Goushi, K.; Ribierre, J.-C.; Adachi, C. Indication of Current-Injection Lasing from an Organic Semiconductor. *Appl. Phys. Express* **2019**, *12*, 061010.
- (13) Liu, D.; De, J.; Gao, H.; Ma, S.; Ou, Q.; Li, S.; Qin, Z.; Dong, H.; Liao, Q.; Xu, B.; Peng, Q.; Shuai, Z.; Tian, W.; Fu, H.; Zhang, X.; Zhen, Y.; Hu, W. Organic Laser Molecule with High Mobility, High Photoluminescence Quantum Yield, and Deep-Blue Lasing Characteristics. *J. Am. Chem. Soc.* **2020**, *142*, 6332–6339.
- (14) Hou, L.; Zhang, X.; Cotella, G. F.; Carnicella, G.; Herder, M.; Schmidt, B. M.; Patzel, M.; Hecht, S.; Cacialli, F.; Samori, P. Optically Switchable Organic Light-Emitting Transistors. *Nat. Nanotechnol.* **2019**, *14*, 347–353.
- (15) Yuan, D.; Sharapov, V.; Liu, X.; Yu, L. Design of High-Performance Organic Light-Emitting Transistors. *ACS Omega* **2020**, 5, 68
- (16) Zhang, X.; Dong, H.; Hu, W. Organic Semiconductor Single Crystals for Electronics and Photonics. *Adv. Mater.* **2018**, *30*, No. 1801048.
- (17) Xie, Z.; Liu, D.; Zhang, Y.; Liu, Q.; Dong, H.; Hu, W. Recent Advances on High Mobility Emissive Anthracene-Derived Organic Semiconductors. *Chem. J. Chin. Univ.* **2020**, 20190650.
- (18) Sundar, V. C.; Zaumseil, J.; Podzorov, V.; Menard, E.; Willett, R. L.; Someya, T.; Gershenson, M. E.; Rogers, J. A. Elastomeric Transistor Stamps: Reversible Probing of Charge Transport in Organic Crystals. *Science* **2004**, 303, 1644–6.
- (19) Zaumseil, J.; Donley, C. L.; Kim, J. S.; Friend, R. H.; Sirringhaus, H. Efficient Top-Gate, Ambipolar, Light-Emitting Field-Effect Transistors Based on a Green-Light-Emitting Polyfluorene. *Adv. Mater.* **2006**, *18*, 2708–2712.
- (20) Gwinner, M. C.; Kabra, D.; Roberts, M.; Brenner, T. J.; Wallikewitz, B. H.; McNeill, C. R.; Friend, R. H.; Sirringhaus, H. Highly Efficient Single-Layer Polymer Ambipolar Light-Emitting Field-Effect Transistors. *Adv. Mater.* **2012**, *24*, 2728–34.
- (21) Li, J.; Zhou, K.; Liu, J.; Zhen, Y.; Liu, L.; Zhang, J.; Dong, H.; Zhang, X.; Jiang, L.; Hu, W. Aromatic Extension at 2,6-Positions of Anthracene toward an Elegant Strategy for Organic Semiconductors with Efficient Charge Transport and Strong Solid State Emission. *J. Am. Chem. Soc.* 2017, 139, 17261–17264.
- (22) Qin, Z.; Gao, H.; Liu, J.; Zhou, K.; Li, J.; Dang, Y.; Huang, L.; Deng, H.; Zhang, X.; Dong, H.; Hu, W. High-Efficiency Single-Component Organic Light-Emitting Transistors. *Adv. Mater.* **2019**, *31*, No. 1903175.
- (23) Park, S. K.; Kim, J. H.; Ohto, T.; Yamada, R.; Jones, A. O. F.; Whang, D. R.; Cho, I.; Oh, S.; Hong, S. H.; Kwon, J. E.; Kim, J. H.; Olivier, Y.; Fischer, R.; Resel, R.; Gierschner, J.; Tada, H.; Park, S. Y. Highly Luminescent 2d-Type Slab Crystals Based on a Molecular Charge-Transfer Complex as Promising Organic Light-Emitting Transistor Materials. *Adv. Mater.* 2017, 29, 1701346.
- (24) Capelli, R.; Toffanin, S.; Generali, G.; Usta, H.; Facchetti, A.; Muccini, M. Organic Light-Emitting Transistors with an Efficiency That Outperforms the Equivalent Light-Emitting Diodes. *Nat. Mater.* **2010**, *9*, 496–503.
- (25) Seo, J. H.; Namdas, E. B.; Gutacker, A.; Heeger, A. J.; Bazan, G. C. Solution-Processed Organic Light-Emitting Transistors Incorporating Conjugated Polyelectrolytes. *Adv. Funct. Mater.* **2011**, *21*, 3667–3672.
- (26) Usta, H.; Sheets, W. C.; Denti, M.; Generali, G.; Capelli, R.; Lu, S.; Yu, X.; Muccini, M.; Facchetti, A. Perfluoroalkyl-Functionalized Thiazole—Thiophene Oligomers as N-Channel Semiconductors in Organic Field-Effect and Light-Emitting Transistors. *Chem. Mater.* 2014, 26, 6542–6556.

- (27) Ullah, M.; Wawrzinek, R.; Nagiri, R. C. R.; Lo, S.-C.; Namdas, E. B. Uv-Deep Blue-Visible Light-Emitting Organic Field Effect Transistors with High Charge Carrier Mobilities. *Adv. Opt. Mater.* **2017**, *5*, 1600973.
- (28) Chen, H.; Xing, X.; Miao, J.; Zhao, C.; Zhu, M.; Bai, J.; He, Y.; Meng, H. Highly Efficient Flexible Organic Light Emitting Transistor Based on High-K Polymer Gate Dielectric. *Adv. Opt. Mater.* **2020**, *8*, 1901651.
- (29) Tomkeviciene, A.; Grazulevicius, J. V.; Volyniuk, D.; Jankauskas, V.; Sini, G. Structure-Properties Relationship of Carbazole and Fluorene Hybrid Trimers: Experimental and Theoretical Approaches. *Phys. Chem. Chem. Phys.* **2014**, *16*, 13932–42.
- (30) Hu, G.; Billa, M. R.; Kitney, S. P.; Kelly, S. M. Symmetrical Carbazole–Fluorene–Carbazole Nematic Liquid Crystals as Electroluminescent Organic Semiconductors. *Liq. Cryst.* **2018**, *45*, 965–979.
- (31) Enriquez-Cabrera, A.; Lacroix, P. G.; Sasaki, I.; Mallet-Ladeira, S.; Farfán, N.; Barba-Barba, R. M.; Ramos-Ortiz, G.; Malfant, I. Comparison of Carbazole and Fluorene Donating Effects on the Two-Photon Absorption and Nitric Oxide Photorelease Capabilities of a Ruthenium-Nitrosyl Complex. Eur. J. Inorg. Chem. 2018, 2018, 531–543.
- (32) Xu, J.; Ji, Q.; Kong, L.; Du, H.; Ju, X.; Zhao, J. Soluble Electrochromic Polymers Incorporating Benzoselenadiazole and Electron Donor Units (Carbazole or Fluorene): Synthesis and Electronic-Optical Properties. *Polymers (Basel, Switz.)* 2018, 10, 450.
- (33) Cai, Z.; Awais, M. A.; Zhang, N.; Yu, L. Exploration of Syntheses and Functions of Higher Ladder-Type  $\Pi$ -Conjugated Heteroacenes. *Chem.* **2018**, *4*, 2538–2570.
- (34) Liao, Q.; Cao, J.; Xiao, Z.; Liao, J.; Ding, L. Donor-Acceptor Conjugated Polymers Based on a Pentacyclic Aromatic Lactam Acceptor Unit for Polymer Solar Cells. *Phys. Chem. Chem. Phys.* **2013**, *15*, 19990–3.
- (35) Poduval, M. K.; Burrezo, P. M.; Casado, J.; López Navarrete, J. T.; Ortiz, R. P.; Kim, T.-H. Novel Thiophene—Phenylene—Thiophene Fused Bislactam-Based Donor—Acceptor Type Conjugate Polymers: Synthesis by Direct Arylation and Properties. *Macromolecules* **2013**, *46*, 9220—9230.
- (36) (a) Spano, F. C.; Silva, C. H- and J-Aggregate Behavior in Polymeric Semiconductors. *Annu. Rev. Phys. Chem.* **2014**, *65*, 477–500. (b) Spano, F. C. The Spectral Signatures of Frenkel Polarons in H- and J-Aggregates. *Acc. Chem. Res.* **2010**, *43*, 429–39.
- (37) Zheng, C.; Zhong, C.; Collison, C. J.; Spano, F. C. Non-Kasha Behavior in Quadrupolar Dye Aggregates: The Red-Shifted H-Aggregate. J. Phys. Chem. C 2019, 123, 3203–3215.
- (38) Terenziani, F.; Painelli, A.; Katan, C.; Charlot, M.; Blanchard-Desce, M. Charge Instability in Quadrupolar Chromophores: Symmetry Breaking and Solvatochromism. *J. Am. Chem. Soc.* **2006**, 128, 15742–55.
- (39) Birks, J. B.; Christophorou, L. G. Excimer Fluorescence Spectra of Pyrene Derivatives. *Spectrochim. Acta* **1963**, *19*, 401–410.